SLAC-J-ICFA-17
December 1998
SLAC-R-648

HOME PAGE

http://www.slac.stanford.edu/pubs/icfa/

ICFA INSTRUMENTATION BULLETIN*

The publication of the ICFA Instrumentation Bulletin is an activity of the Panel on Future Innovation and Development of ICFA (International Committee for Future Accelerators).

Volume 17

• Fall 1998 Issue

* Supported by the Department of Energy, contract DE-AC03-76SF00515.

ICFA INSTRUMENTATION BULLETIN

The publication of the ICFA Instrumentation Bulletin is an activity of the Panel on Future Innovation and Development of ICFA (International Committee for Future Accelerators). The Bulletin reports on research and progress in the field of instrumentation with emphasis on application in the field of high-energy physics. It encourages issues of generic instrumentation.

Publisher : Stanford Linear Accelerator Center
SLAC Publications Department
Stanford, CA 94309, U.S.A.

Editor : J. Va'vra

Web Technical Advisers : J. Schwiening and T. Pavel

http://www.slac.stanford.edu/pubs/icfa/

Cover: The illustration depicts L. J. Waghenaer's marine atlas, "The Mariner's Mirror," published in 1588. Lucas Janszoon Waghenaer was born in Holland in the 1530s. He became a famous ship pilot in his time. In 1584, he published the atlas ("Spieghel der Zeevaerdt") which was greatly valued among mariners for centuries. This was not due only to the map content, but also to the detailed knowledge of navigation techniques of that time. The atlas, as it appears on our page, is the same one used for the Dutch to English translation.

Table of Contents

1999 Conference List

- VIII ICFA School on Instrumentation in Elementary Particle Physics
  June 28-July 10, 1999, University of Istanbul, Istanbul, Turkey,
  http://icfa99.istanbul.edu.tr.

- Second Conference on New Developments in Photodetection, BEAUNE '99
  21-25 June, 1999, Beaune, France.

- ITP Conference on Magnetic Phenomena in Novel Materials and Geometries,
  16-20 August 1999, Santa Barbara, CA, U.S.A.

- The 5th International Conference on Position Sensitive Detectors,
  September 1999, London, England.

- The 46th National Symposium of the American Vacuum Society,
  8-22 October 1999, Seattle, WA, U.S.A.

- The 11th International Workshop on Room Temperature Semiconductor X Ray and
  Gamma Ray Detectors and Associated Electronics,
  11-15 October 1999, Vienna, Austria.

- The 11th U.S. National Synchrotron Radiation Instrumentation Conference (SRI99),
  13-15 October 1999, Stanford, CA, U.S.A.

- The IEEE Nuclear Science Symposium and Medical Imaging Conference,
  26-30 October 1999, Seattle, U.S.A.

- The 7th International Conference on Instrumentation for Colliding Beam Physics (INSTR99),
  5-19 November 1999, Hamamatsu, Japan.

99-03-074

High-Gain operation of GEM in pure argon

A. Bressan[a], A. Buzulutskov[b*], L. Ropelewski[a], F. Sauli[a], and L. Shekhtman[b]

[a] CERN, Geneva, Switzerland
[b] Budker Institute of Nuclear Physics, Novosibirsk, Russia

Abstract

We study the operation of the Gas Electron Multiplier (GEM) in pure Ar, in comparison to that in Ar-CO_2 mixture. In pure Ar, high GEM gains, of above 700 and 3000 for single and double GEM structures correspondingly, have been obtained. It is observed that the GEM effective gain and its charging-up are strongly affected by electric field values above and below the GEM. Applications to the development of non-ageing gas photomultiplier are discussed.

1. Introduction

It is generally accepted that gas devices cannot properly operate in a multiplication mode in noble gases, unless some quantity of the quenching gas (mostly organics) is added. Indeed, many years ago it was recognized that the maximum gas gain achievable in pure noble gases is rather low, due to a very early onset of secondary avalanche processes [1]. In particular, in pure Ar the gas amplification factor does not exceed a few hundreds in proportional counters [2,3] and a few tens in parallel-plate chambers [4,5].

The poor quenching properties of the noble gas molecule are due to the fact that it is monoatomic. This characteristic however is very useful if one is interested in non-ageing detectors. In contrast to molecular gases, for monoatomic gases, nothing can decompose and thus induce ageing. Nonageing gas fillings are of primary importance for the development of the gas photomultipliers [5-8], where even tiny amount of chemically active molecules created in an avalanche can destroy the sensitive photocathode layer. In particular, the stability of Ar-filled photodiodes was proved by exploiting a very large number of them in sound film reproduction [4].

During the last two years, a new gas device with internal amplification is being intensively developed: the Gas Electron Multiplier (GEM) [9-13]. GEM is a thin kapton foil metal-clad on both sides and perforated by a high density of micro-holes, inside which gas amplification occurs. It has been recently conjectured [13] that GEM can effectively operate in pure noble gases, since the quenching properties of the filling gas

* Corresponding author. E-mail: buzulu@inp.nsk.su.

are less important compared to other gas amplification devices. Moreover, it was shown that the GEM operation in pure Xe almost does not differ from that in Xe-CO_2.

The possible reason is the effect of the avalanche confinement in GEM micro-holes [13]. One aspect of the effect is obvious: GEM is basically a multisegmented device, with suppressed feedbacks between holes. The second aspect is that, due to the high dipole field formed inside the hole [10], the avalanche is externally quenched when developing too far from the hole axis. Therefore, no matter what gas is used, the avalanche will be confined within a small space of a dimension of a few tens of microns, even at high gains, preventing the development of the discharge. In the present work we study the GEM operation in pure Ar, and compare to that in Ar-CO_2 mixture. We show that rather high gains are reached both for single and double GEM structures. We also investigate the effect of the electric field above and below GEM on its effective gain and charging-up.

2. Experimental Setup and Procedure

All GEM devices investigated had a similar basic structure: 5mm copper electrodes were plated on 50μm Kapton; the diameter of the holes on the metal and the Kapton were 80 and 50μm, respectively; the pitch was 140μm; the active area was 10×10cm^2. Either a single or double GEM structure was coupled to a printed circuit board (PCB) with a 200μm pitch strip pattern, used as a readout element (Fig.1).

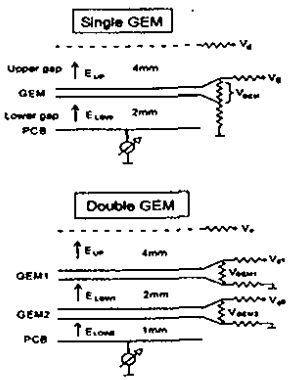

Figure 1. Schematics of a single and double GEM assembly with the appropriate notations.

For the single GEM assembly, the upper and lower gaps were 4 and 2 mm, correspondingly. For the double GEM assembly, the distance between GEMs was 2 mm and the upper and lower gap were 4 and 1 mm, correspondingly. The detector was flushed at atmospheric pressure with pure Ar or Ar-CO_2 (70-30).

Depending on the measurement to be performed, the PCB was grounded through a picoammeter or amplifier input. The high voltage was supplied to GEM electrodes through a resistive voltage divider. For the single GEM, the electric field below GEM, E_{LOW}, was proportional to the voltage applied across the GEM (GEM voltage, V_{GEM}): E_{LOW} = (4, 5 or 10 kV/cm)×(V_{GEM}/400V). The electric field above GEM, E_{UP}, was fixed.

In a symmetrical mode of operation of the double GEM, $V_{GEM1} = V_{GEM2} = V_{GEM}$ and the electric fields below each GEM were equal: $E_{LOW1} = E_{LOW2}$ = (4kV/cm)×(V_{GEM}/400V). In the asymmetrical mode of operation, the voltage on the first GEM was fixed, the lower field of the second GEM was the same as before, while the field bewteen GEMs was weaker, varying between 2.4 and 3.4 kV/cm.

The detector was irradiated with a 8 keV X-ray beam over an area of ~40cm^2 with a rate in a range between 10^1 and 10^4 mm^{-2}s^{-1}. In the pulse-height measurements, the exposed area was reduced to 2 mm^2 to prevent overloading of the amplifier.

The effective GEM gain was determined measuring either the pulse-height, with the help of a charge-sensitive preamplifier (integration time is 300ns), or the current from the PCB. Both techniques gave similar results. The absolute gain calibration was done at a point where both the current and the counting rate could be recorded simultaneously, assuming the initial charge in the upper gap generated by an X-ray conversion to be well known. The maximum gain is defined as the gain at the highest voltage at which there are still no micro-discharges during at least 1 min. The accuracy of the absolute gain values measured is estimated to be 20%.

3. Results

In a single GEM assembly, a large signal has been detected in pure Ar, with no afterpulses seen even at the highest gains. Figure 2 shows the GEM gains as a function of GEM voltage measured in Ar-CO_2 and in pure Ar at different rates; the last points correspond to the maximum safe gains obtained at a given rate. The data sets were measured at optimized upper fields E_{UP} and at different lower fields E_{LOW}.

One can see that the maximum gain attainable in pure Ar is about 700 at a rate of 10^2 mm^{-2}s^{-1} in a large exposed area. The maximum gain drops down to 500 when increasing the rate by an order of magnitude. On the other hand, it can approach 1000 reducing the exposed area and slightly increasing the lower field, from (4 to 5 kV/cm)× (V_{GEM}/400V). This should be compared to 3000, the maximum gain value obtained in Ar-CO_2 at a similar ratio of lower field to GEM field.

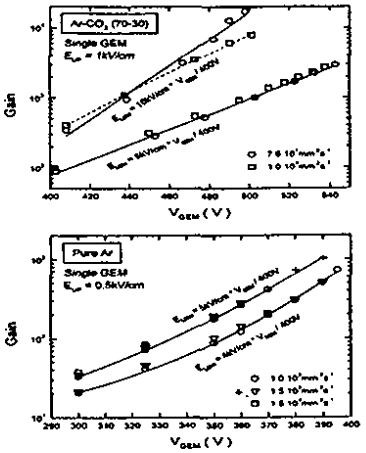

Figure 2. Effective gain of a single GEM as a function of GEM voltage measured in Ar-CO_2 and in pure Ar at different rates and different E_{LOW}. The exposed area of the detector was 40 cm^2, except for the last two data points in the Ar plot (cross symbols) where it was reduced to 2 mm^2.

It has been recently understood [10,11] that the values of the upper and lower electric fields play a crucial role on the effective GEM gain, i.e., on the sharing between the charge captured into GEM holes and the one transfered, after amplification, to the lower gap. This fraction is a function of the ratios E_{UP}/E_{GEM} and E_{LOW}/E_{GEM} (here E_{GEM} is the average field in GEM holes), of the electron diffusion and of the GEM geometrical transparency. Indeed, the higher the ratio E_{LOW}/E_{GEM}, the larger fraction of charge is transferred from holes into the lower gap. Conversely, the higher the ratio E_{UP}/E_{GEM}, the larger fraction of charge is lost due to termination of the field lines on the upper GEM electrode.

The last point is illustrated in Fig. 3, showing the relative gain as function of the upper field: in pure Ar the optimal value of E_{UP} is below 0.5 kV/cm. In Ar-CO_2 , the maximum value of E_{UP} is significantly larger: about 1.5 kV/cm [10]. The difference can be explained by the lower GEM operation voltage and probably by larger electron diffusion in pure Ar.

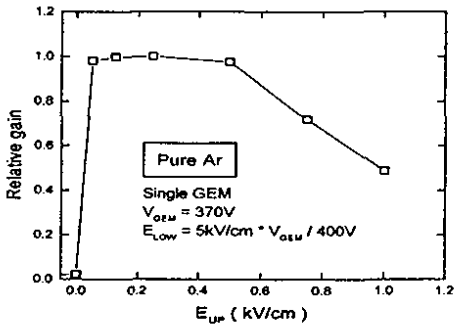

Figure 3. Relative gain of a single GEM in pure Ar as a function of the electric field in the upper gap.

At too high values of the lower field, the lower gap starts to operate in a parallel-plate amplification mode. Though providing an additional gain, the parallel-plate mode results in two negative effects: gain nonuniformity over the area, and the charging-up of GEM. The latter is induced by a positive charge accumulation on the lower, bare kapton side due to ion feedback. Charging-up manifests itself in gain increase at low rates, due to enhancement of the local field in GEM holes, and in gain decrease at high rates, due to reduction of the lower field.

This is illustrated in Fig. 2. At $E_{LOW} \leq$ (5 kV/cm)×(V_{GEM}/400V), below parallel-plate multiplication, there is no dependence of gain on the rate in both Ar-CO_2 and Ar. This is however not the case when increasing the lower field by a factor of 2 (see Ar-CO_2 plot). Due to the parallel-plate mode contribution, the gain drop can be as large as 50% at a rate of 10^4 compared to that of 10^2 mm^{-2} s^{-1} .

We observed the effect of charging-up in pure Ar when the absolute value of the lower field reached 4.9 kV/cm, the value at which an avalanche multiplication starts in Ar [14,15]. Figure 4 shows the gain stability studied at the same GEM voltages but at different lower fields. One can see that while at E_{LOW} = 3.95 kV/cm the gain is stable, at

E_{LOW} = 4.94 kV/cm it grows with time until sparking. The spark discharge neutralizes a positive charge accumulated on GEM and initiates the next charging-up cycle.

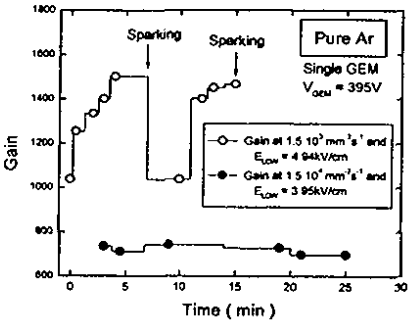

Figure 4. Effect of GEM charging-up in pure Ar. Shown is the GEM gains as a function of time measured at the same GEM voltages, but at different electric fields in the lower gap. The exposed area is 2 mm^2.

Further increase of the maximum gain was obtained in a double GEM structure (see Fig. 5). In a symmetrical operation mode, the maximum gain in pure Ar was about 3000, which should be compared to a value of 20000 obtained in Ar-CO_2. Even higher gains, of above 4000, are reached if to operate in the asymmetrical mode, where the voltage on the second GEM is higher than on the first.

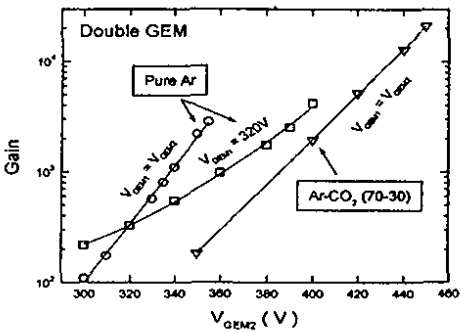

Figure 5. Effective gain of a double GEM in a symmetrical ($V_{GEM1} = V_{GEM2}$) and asymmetrical (V_{GEM1} is fixed) operation mode as a function of the voltage of the second GEM, measured in Ar-CO_2 and in pure Ar. The exposed area is 2mm^2; the rate is 10^3 mm^{-2} s^{-1}. The upper fields are 1 and 0.4 kV/cm for Ar-CO_2 and pure Ar, correspondingly.

Rather satisfactory energy resolution in both single and double GEM was obtained in pure Ar. For example, Fig. 6 shows the pulse-height spectra for 8 keV X-rays measured in a double GEM. Its energy resolution in Ar (FWHM=23%) corresponds to that in Ar-CO_2.

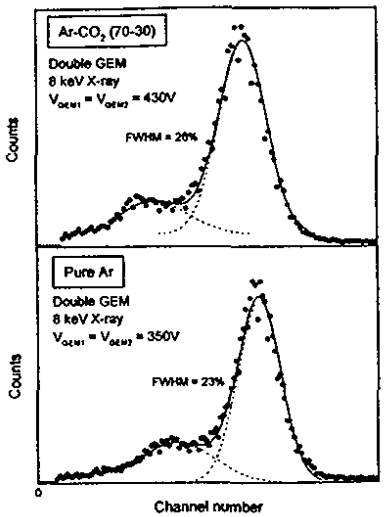

Figure 6. Pulse-height spectra in a double GEM for 8 keV X-rays, measured in Ar-CO_2 and pure Ar at effective gains of about 8000 and 2000, correspondingly. Other conditions are the same as those of Fig. 5.

4. Summary

In conclusion, we have demonstrated that rather large GEM gains, above 700, can be obtained in pure Ar in a single GEM, and very large gains, above 3000, in a double GEM, with reasonable energy resolution. This is exceptional for a proportional counter, and is probably a consequence of the avalanche confinement in GEM micro-holes.

It should be remarked that the GEM electrodes used in the present study had been previously used in a systematic investigation of discharge limits, and might here been slightly damaged. Therefore one would expect, that for a pristine GEM, the nominal maximum gain in Ar can be even higher, supposingly by a factor of 2-3.

We also expect that the further gain increase might be possible in Xe, provided that a similar tendency is observed in its mixtures with CO_2 .

An important observation is that optimal electric fields in Ar are significantly lower compared to those in Ar-CO_2. In order to avoid charge losses and charging-up, the electric fields should be less than 0.5 kV/cm and 4.9 kV/cm above and below the GEM correspondingly. This is an outcome of the lower GEM operation voltage and the earlier beginning of the parallel-plate mode contribution.

The results obtained can find application mostly in the field of nonageing gas devices. In pure noble gases, the electron drift velocity is relatively small and the diffusion is large. Consequently, the Ar-filled devices may not be applied to track detection at high rates because of the large charge collection time. However, they may be relevant to the development of the gas photomultiplier where the parallax of the charge conversion point is absent. In particular, the gas photon detector, consisting of a series of GEMs coupled to a solid photocathode and operated in pure Ar, Kr, or Xe, could be sealed, would be very long-lasting, and not subjected to ageing. The lifetime of such gas photomultipliers can even exceed that of the conventional vacuum phototubes, due to the lower ion energy in a gas medium compared to vacuum, and thus, less effect of the ion bombardment of the photocathode.

References

[1] E. Fünfert and H. Neuert, Zahlrohre und Szintillationszähler, (Verlag, Karlsruhe, 1959), and references therein.

[2] L. Colli, N. Facchini and E. Gatti, Phys. Rev. 80 (1950) 92.

[3] F.Sauli, Principle of operation of multiwire proportional and drift chambers, in «Experimental Techniques in High Energy Physics,» ed. T. Ferbel, (Addison-Wesley, 1987), and references therein.

[4] A.H. Sommer, Photoemissive Materials, (Krieger, Huntington, 1980), and references therein.

[5] G. Charpak, W. Dominik, F. Sauli and S. Majewski, IEEE Trans. Nucl. Sci. 30 (1983) 134.

[6] V. Peskov and E. Silin, Nucl. Instr. Meth. A 367 (1995) 347.

[7] A. Buzulutskov, E. Shefer, A. Breskin, R. Chechik and M. Prager, Nucl. Instr. Meth. A 400 (1997) 173.

[8] E. Shefer, A. Breskin, A. Buzulutskov, R. Chechik and M. Prager, Composite

photocathodes for visible photon imaging with gaseous photomultipliers, Preprint WIS-98/7/Apr.-DPP, presented at the 1998 Vienna Wire Chamber Conf., to be published in Nucl. Instr. Meth. A.

[9] F. Sauli, Nucl. Instr. Meth. A 386 (1997) 531.

[10] R. Bouclier, W. Dominik, M. Hoch, J.C. Labbe, G. Million, L. Ropelewski, F. Sauli, A. Sharma and G. Manzin, Nucl. Instr. Meth. A 396 (1997) 50.

[11] J. Benlloch, A. Bressan, M. Capeáns, M. Gruwé, M. Hoch, J.C. Labbé, A. Placci, L. Ropelewski and F. Sauli, Further developments of the Gas Electron Multiplier (GEM), Preprint CERN-EP/98-50, presented at the 1998 Vienna Wire Chamber Conf., to be published in Nucl. Instr. Meth. A.

[12] R. Chechik, A. Breskin, G. Garty, J. Mattout, F. Sauli and E. Shefer, First results on the GEM operated a low gas pressures, Preprint WIS-98/08/MAY.-DPP, presented at the 1998 Vienna Wire Chamber Conf.'98, to be published in Nucl. Instr. Meth. A.

[13] A. Bondar, A. Buzulutskov, F. Sauli and L. Shekhtman, High and low pressure operation of the gas electron multiplier, presented at the 1998 Vienna Wire Chamber Conf, to be published in Nucl. Instr. Meth.

[14] L.B. Loeb, Basic processes of gaseous electronics, (University of California Press, Berkley, 1961).

[15] B. Sitar, G.I. Merson, V.A. Chechin and Yu.A. Budagov, Ionization measurements, (Springer-Verlag, Berlin, 1993).

INFRARED EMISSION: A NEW POSSIBLE APPROACH TO PARTICLE DETECTORS

G. Carugno*

INFN, Sezione di Padova, Via Marzolo 8, Padova, Italy

Abstract

A brief review on the infrared concepts and photodetectors will be summarized. Emission of infrared photons has been observed in an ionization chamber filled with standard gases and some results are reported. Light produced by the electron drifting in the gaseous media has also been observed. Results are presented as a function of the electric drift field.

1. INTRODUCTION

Few data are available in the literature about the correlation between the ionization phenomena and the infrared (I.R.) signals (the typical range of the I.R. photon energy is between 0.01 and 1 eV).

The reported experimental data [1] only concerns the area near the I.R. region (≤ 900nm). This was possible using a GaAs photomultiplier (Q.E. = 20% up to 900 nm). Studying proportional scintillation in noble gases, some groups [2] stated a possibility of further emission in the wider I.R. region. In fact, an incomplete energy balance in the photon emission process was seen.

Another unsolved question is related to the energy resolution in cryogenic noble liquid detectors, and the possibility of some energy output in the I.R. channel [3], according to a dimeric deexcitation. This is why we started our measurements hoping that some I.R. processes occur due to prompt or proportional scintillation. We also noticed that the drifting electron energy under the electric field ($E_{electron} = e * \overline{E} * \lambda \approx 0.2$ eV), and the I.R. photon energy yield the same order of magnitudes.

We speculate that due to the low energy quanta involved, the energy resolution can be improved with a high I.R. light yield scintillator

In the last few years, after the end of the cold war, good photodetectors have been made available to detect photons in the infrared region. The progress in I.R. technology has been largely used in astrophysical measurements.

For our purpose there are two kinds of useful I.R. sensors: photovoltiac and photoconductive. They can reach, under a controlled and cooled environment, a quantum

* E-mail address: carugno@pdinfn.it.

efficiency of up to 80% at a 10 μm wavelength, with a possibility of detecting a few thousands of I.R. photons.

The I.R. materials, optics [4], and detectors [5] are available from many vendors. One of the limits affecting this field is the high cost of these devices compared to those devices which are sensitive in the visible wavelength region.

Due to the blackbody radiation representing a major drawback for I.R. particle detectors, the reader is reminded in Chapter 2 of some of the concepts on I.R. radiation and the present state-of-the-art in I.R. materials, detectors and handling methods. In Chapter 3 and 4, we present our measurements. In Chapter 5, we will consider the possible directions of future research in the field of high-energy detectors.

2. INFRARED PRIMER GUIDE

2.1. Infrared Radiation

The I.R. wavelength region ranges from 0.75 μm (1.65 eV) to a few 100μm (≈ MeV). The I.R. region is usually subdivided in three regions: near (0.75÷3 μm), middle (3÷6 μm), and far (6÷15μm), respectively. Each region corresponds to different kinds of photodetectors.

Objects at a temperature higher than 0 °K radiate due to the blackbody radiation. There are three main formulas governing the blackbody radiation:

(1) Planck's blackbody radiation law

$W_\lambda = c_1 \ \lambda^{-5} \ [\exp (c_2 / \lambda T) - 1]^{-1}$ [Watt / cm^2 μm]

T = absolute temperature [°K]; λ = wavelenght [μm],

$c_1 = 3.74 * 10^4$ [Watt μm^4 / cm^2] $c_2 = 1.43 * 10^4$ [μm °K].

(2) Stefan-Boltzmann law

$W = \sigma T^4$ [W / cm^2] $\sigma = 5.66 * 10^{-12}$ [Watt/cm^2 °K^4].

(3) Wien displacement law

$\lambda_{max} * T = 2897$ [μm °K].

Figures 2.1 and 2.2 show the Planck radiation law expressed in terms of spectral radiant photon emittance.

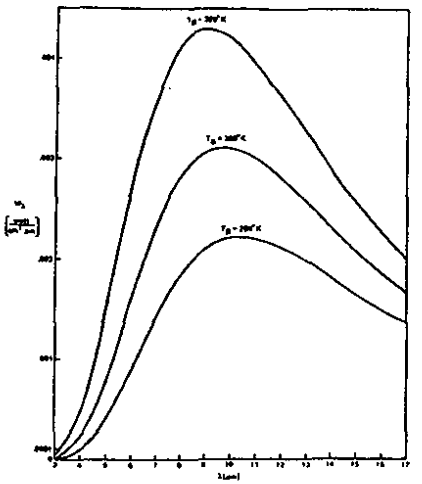

Figure 2.1. Planck's law for spectral radiant emittance at three background temperatures T_B.

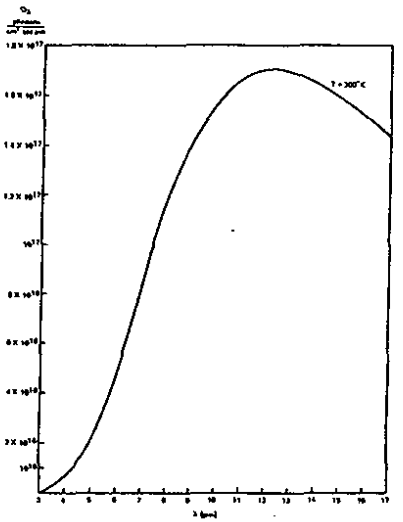

Figure 2.2. Planck's law for spectral photon emittance at a background temperature of 300°K.

The objects are not usually ideal blackbody sources; i.e., the emissivity of the material must be taken into account (W' = εW). Highly reflective metallic surfaces or I.R. transparent materials typically have a very low emissivity (see Figure 2.3 for details).

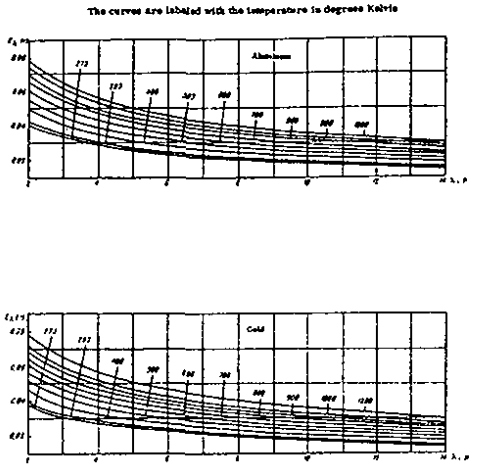

Figure 2.3. Spectral emissivity ε of aluminum and gold in the infrared region.

A huge number of photons emitted from a blackbody source per cm^2/sec makes it difficult to detect transient I.R. signals. Cooling down the entire system (detector + emitting material) helps. For example, the emission peak wavelength of 10 μm at 270°K shifts down to about 50 μm at 77°K, while the overall photon flux decreases from 10^{18} photons/cm^2/s down to 10^{11} photons/cm^2/s.

Another possibility to reduce the continuous blackbody emission is to select a particular I.R. line using very low bandwidth filters. This can decrease the background photon flux by many orders of magnitude.

2.2. Optical Materials

Another useful I.R. characteristic is the larger wavelength with respect to the visible one, which considerably decreases the scattering through the media.

The I.R. transmission through the atmosphere involves absorption in well-defined wavelength ranges due to H_2O, O_2, and CO_2 molecules, see Figure 2.4 and Ref. 6. Care must be taken in choosing the optical transmitting material and the presence of pollutants on the surfaces.

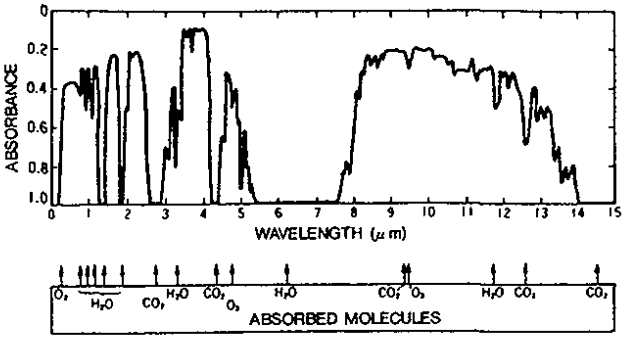

Figure 2.4. Atmospheric absorption above seawater.

The common materials used for I.R. optics such as lenses or windows are shown in Figure 2.5. The degree of transmission for these materials depends on the refractive index[6]. It can easily reach almost 100% with the help of antireflection coating as shown in Figure 2.6 for the germanium window.

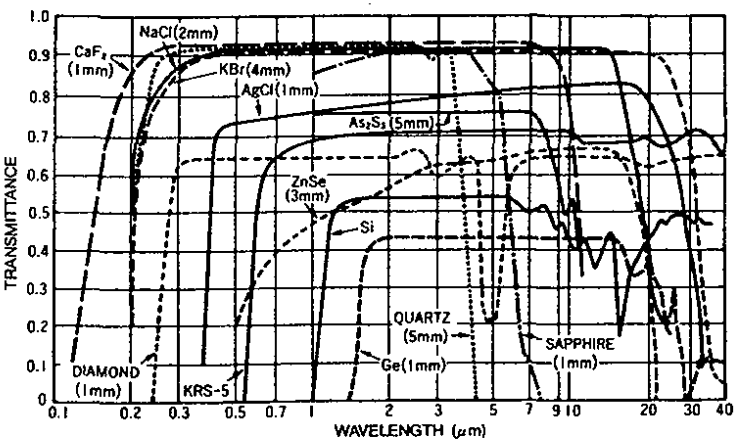

Figure 2.5. Transmittance of optical materials in the infrared region.

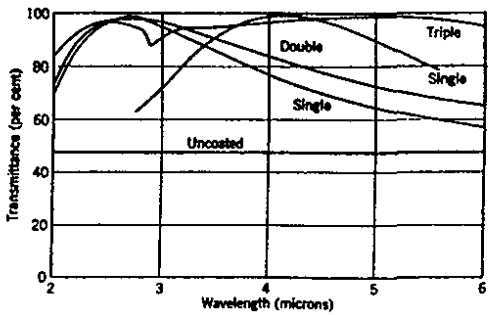

Figure 2.6. Transmittance of a germanium plate with and without antireflection coating.

Aluminum or gold-coated mirrors have a reflectivity of 99%. By means of I.R. emission lines, it is possible to use coated surfaces, e.g., the Febry-Perot cavity in order to have reflectivity as high as 99.99%.

2.3. I.R. Photodetectors

The most suitable detectors for our purpose are the quantum type [7]. The electrons, excited by the I.R. photons in the conduction band, give rise in some semiconductors a detectable current.

Because of the low photon energy, typically ~0.1 eV, it is necessary to cool down the detector to reduce the thermally excited currents in the semiconductor. Recently, Hamamatsu Co. marketed a cooled photomultiplier extending the photocathode quantum efficiency up to 1.7 μm. Most of the detectors are specially packaged to decrease the field of view angle (FOV) in order to reduce the background photons from the blackbody radiation and to optimize the level of the signal. Accurate measurements of low light level signals are made possible using a heterodyne detection method to suppress the blackbody background. This technique allows to detect signals as low as 10^{-20} W/Hz [8].

The glossary of I.R. detector technology takes into account the blackbody background because in these systems both the room temperature environment and the main phenomenon to be detected are normally involved. Such photodetectors are Background Limited Infrared Photo-detection "BLIP" limited.

The three main parameters characterizing the I.R. detectors are Responsivity (R), Noise Equivalent Power (NEP), and the normalized Detectivity (D*) [6]. The Responsivity (R) is the output current or voltage per watt. It is detector dependent when noise is not considered;

$$R = \frac{S}{P\,A} \quad (A/W)_{P.V.} \text{ or } (V/W)_{P.C.},$$

S = Signal output (A) or (V); P = Incident power/cm^2 (W/cm^2),

A = Detector area (cm^2).

The Equivalent Power (NEP) sets the detection limit of the detector, and it is expressed in (W/Hz $^{1/2}$):

$$NEP = \frac{P.A}{S/N\Delta f^{1/2}} = \frac{N}{R.\Delta f^{1/2}},$$

N = noise output (V) or (A),

Δf = noise bandwidth (Hz).

The Detectivity (D*) allows the possibility to make a comparison between different detectors; it is normalized to 1 cm^2 and 1 Hz amplifier bandwidth:

$$D^* = \frac{S/N\Delta f^{1/2}}{P.A^{1/2}} = \frac{A^{1/2}}{NEP} \quad (\text{cm Hz}^{1/2}/\text{W} = \text{Jones}).$$

The D* values are quoted for a given measurement condition depending on the temperature of the radiant source, chopping frequency, and amplifier bandwidth. The D* limit, computed from theoretical considerations [6] only taking into account the I.R. blackbody background, for photo-voltaic (PV) and photoconductive (PC) detectors:

$$D^*_{(PV)} = \frac{\lambda}{hc}\,\xi^{1/2}/(2Q)^{1/2} \quad (\text{cm Hz}^{1/2}/\text{W}),$$

$$D^*_{(PC)} = \frac{\lambda}{2hc}\,\xi^{1/2}/Q^{1/2} \quad (\text{cm Hz}^{1/2}/\text{W}),$$

where λ is wavelength, ξ is the quantum efficiency, h is the Planck constant, c is the speed of light and Q is the flux of background radiation.

As shown in Figure 2.7, the manufacturers quote the Detectivity of their products for the BLIP conditions to 300 °K radiant source, and FOV of 180°. Table 1 shows the typical Detectivity values for quantum type detectors [5]. The I.R. detectors currently used are BLIP limited. Therefore, the Detectivity can be increased by many orders of magnitude when cooling the external environment of the detector. For example, the Detectivity value of the InSb semiconductor at 5 μm with ξ = 70%, FOV = 180°, radiant source at 500°K, chopper frequency at 1200Hz, and 1Hz amplifier bandwidth is 10^{10}. If the radiant environment is cooled down to 77°K, its Detectivity increases to 10^{15}.

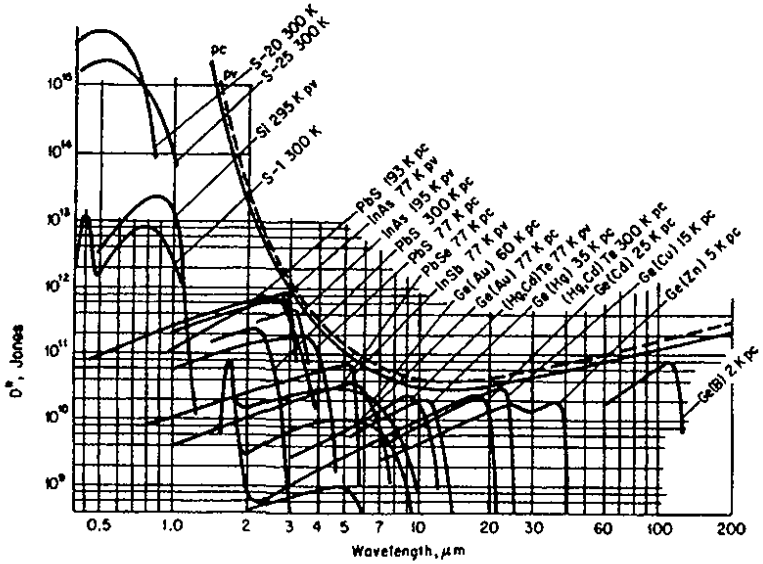

Figure 2.7. Detectivity for various infrared photodetectors (the BLIP curves are plotted for 300°K, 180° FOV.

Table I - Quantum Types Infrared Photodetectors and Their Characteristics.

Quantum type detector	Intrinsic type detector	Photo-conductive type	PbS	1.0 to 3.6	300	D* (500,600,1)=1×10⁹	200
			PbSe	1.5 to 5.8	300	D* (500,600,1)=1×10⁸	3
			HgCdTe	2 to 12	77	D* (500,1000,1)=2×10¹⁰	1
		Photo-voltaic type	Ge	0.8 to 1.8	300	D* (λp,1000,1)=1×10¹¹	2
			InGaAs	0.7 to 1.7	300	D* (λp,1000,1)=5×10¹²	0.0003
			InAs	1 to 3.1	77	D* (500,1200,1)=1×10¹⁰	1
			InSb	1 to 5.5	77	D* (500,1200,1)=2×10¹⁰	1
			HgCdTe	2 to 16	77	D* (500,1000,1)=1×10¹⁰	0.005
	Extrinsic type detector		Ge:Au	1 to 10	77	D* (500,900,1)=1×10¹¹	0.05
			Ge:Hg	2 to 14	4.2	D* (500,900,1)=8×10⁹	0.05
			Ge:Cu	2 to 30	4.2	D* (500,900,1)=5×10⁹	0.05
			Ge:Zn	2 to 40	4.2	D* (500,900,1)=5×10⁹	0.05
			Si:Ga	1 to 17	4.2	D* (500,900,1)=5×10⁹	0.05
			Si:As	1 to 23	4.2	D* (500,900,1)=5×10⁹	0.05

I.R. detectors have sensitive surfaces of up to 1 cm^2. It is possible to increase the surface by a factor of 20 or more with special lenses [7]. I.R. sensitive CCD detectors are also available on the market, with wavelengths of up to ~10 μm.

Photoconductive devices are useful for R&D purposes; however, they are slow devices (switch mode) requiring the light pulse time to be higher than the carrier's lifetime; typically at 100 nsec.

We started our measurement with a MCT PC photodetector. Our MCT detector [9] has the following characteristics: working temperature = 77°K, FOV = 60°, detector area = 1 mm^2, Responsivity = 5000 V/W, NEP = $pW/Hz^{1/2}$, risetime = 0.5 μsec, D* (500, 1000, 1) = 4.10^{10} ($cmHz^{1/2}/W$), $Q_{BLIP} \approx 10^{18}$ photons/cm^2/s (300°K), and infrared window = ZnSe. The overall spectral response is shown in Figure 2.8. The maximum wavelength response is about 12 μm (5000 V/W).

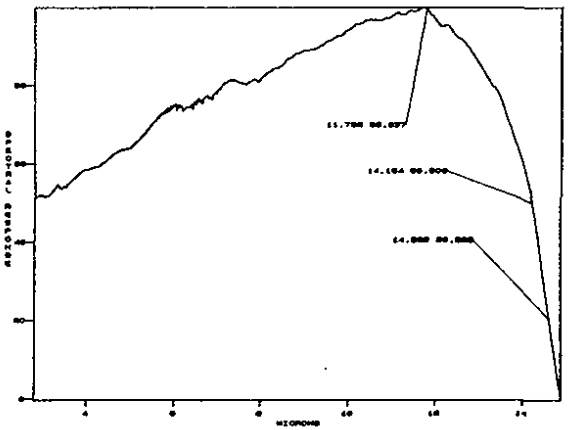

Figure 2.8. MCT P.C. photodetector response in the infrared sensitive region.

3. INFRARED SCINTILLATION IN THE GASEOUS MEDIA INDUCED BY IONIZING MEDIA

We started our investigation looking at standard gaseous systems used to fill an ionization chamber (I.C.). The experimental setup is shown in Figure 3.1.

Protons of 4 MeV from the Legnaro Van der Graaf facility (INFN Nat. Lab.) entered the I.C. The continuous proton beam was chopped with a rotating wheel, generating a time window of about 100 μs every msec, and $10^5 \div 10^6$ protons were contained in each window. The protons entered the I.C. through two 10 μm Mylar windows, and were stopped and measured in the Faraday cup. The approximate energy release per proton in the I.C. at N.P.T was of the order of a few hundred keV. The I.R. sensor (see Fig. 3.1) was placed perpendicularly relative to the beam direction. The solid angle covered by the sensor was ~10^{-3}. The I.C. was made from two metallic plates, 2 cm apart and a diameter of 2 cm. The

one closest to the sensor was made of wires with 1 mm spacing. The cell was rated up to 6 bars. The optical coupling between the I.R. sensor and the I.C. was realized via a ZnSe window. The transmitting wavelength was higher than 750 nm. The ZnSe material is not wave shifting, and stops the known UV scintillation emission [9] from the noble gases.

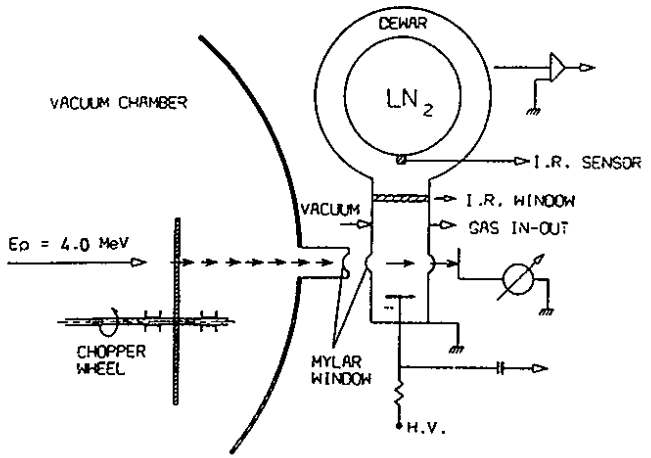

Figure 3.1 - Schematic view of the experimental apparatus (not to scale).

The following gases were tested: He, Ar, Kr, Xe, CO_2, CH_4, and N_2. Some of them are known to be transparent to I.R. radiation (noble gases and N_2). The scintillation was clearly seen only with the noble gases. Helium gave a weaker signal compared to the others. The I.R. emission phenomenon seems to be independent from pressure conditions. The power detected on the I.R. sensor was at a level of a few μW. Our study focused on Argon gas in the pressure ranges from 0.2 to 5.5 bar. A typical I.R. signal from the MCT detector is shown in Figure 3.2.

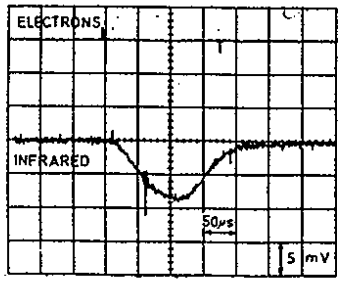

Figure 3.2. Infrared scintillation signal for Argon gas (T = 290°K, P = 1.7 bar). No electron current signal is present (ΔV = 0 in the I.C. electrodes).

In order to understand the emission spectra, we used materials with different transmission characteristics between the I.R. sensor and the I.C. window. The result is the emission wavelength centered between 1 and 2 μm. These measurements are very preliminary and we are planning to make a systematic study with a spectrophotometer to measure more precisely the emitting wavelength. This emission line is probably related to dimeric deexcitation of the Ar_2 [10] molecule formed by ionization. If this is the case, the Xenon should emit around 2μm [11]. We have compelling reasons to believe that scintillation is also present in the liquid phase. We are preparing a cryogenic test cell to be irradiated with an electron beam to look for the I.R. radiation. As stated before, the cryogenic environment reduces dramatically the blackbody background. This gives rise to the possibility of using simple Ge or InGaAs photodiodes in the case of liquid Argon. We intend to look at other materials, liquid and solid, emitting in the I.R. wavelength region.

4. INFRARED EMISSION BY DRIFTING ELECTRONS IN GAS

We noted that the I.R. signal was increased in all noble gases after switching on the electric field in the I.C. In Nitrogen, the I.R. signal, which was not seen in the "prompt mode," appeared when the drift-field was applied. The increase in the I.R. signal is clearly visible in Figure 4.1 for Argon gas. The dependence of the I.R. amplitude on the voltage applied to the I.C. for Argon at 5 bars is shown in Figure 4.2. In the same figure, we show the collected charge as a function of the applied voltage. It was possible to remove the prompt scintillation light by placing a filter between the sensor and the window. The light emitted during the electron drifting was above 2 μm wavelength.

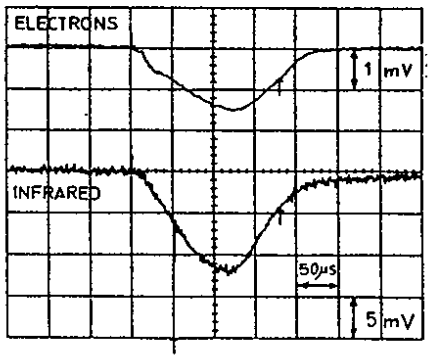

Figure 4.1. Electron current signal (ΔV = + 1500) and infrared signals (prompt + electron drift superimposed).

The mechanism involved in infrared emission is different from the prompt scintillation. The emission light created by the drifting electrons may be related to some excitation of the gas. The onset of such phenomena can be observed at very low electric fields (see Figure 4.2). Up to now, we have not succeeded in understanding whether this emission is continuous or a line spectrum.

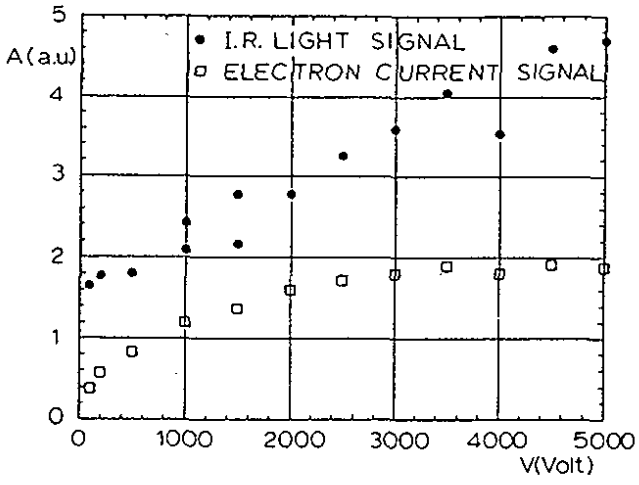

Figure 4.2. Current and I.R. light signal (arbitrary units) vs voltage applied to ionization chamber.

As seen in Figure 4.3, the drifting electrons seem to have excited the Nitrogen molecules in vibrational states, whose lifetime is of the order of a millisecond. This would support the idea of line emission.

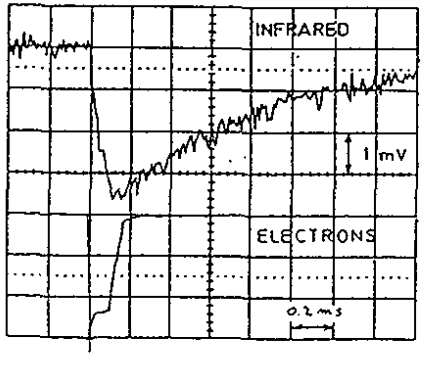

Figure 4.3. Electron current and I.R. light signal in Nitrogen.

The drifting emission in the noble gases seems to be quite efficient and doesn't show any decrease at higher pressure.

The measurements we have obtained are considered preliminary. The investigation can be extended using materials where electrons show high mobility.

5. SUMMARY AND PERSPECTIVES

1. As mentioned above, the data are preliminary and more systematic work is needed.
2. A spectral analysis of the emitted light needs to be measured to explain the mechanism in the prompt and electron drift mode.
3. The light yield of the two emitting modes seem high.
4. There are good reasons to investigate the I.R. scintillation in cryogenic noble liquids.
5. We are searching for the new I.R. scintillator materials (solid, high Z, high light yield) to increase the energy resolution in gamma detection. Possibly, these materials can be found in binary low-band gap semiconductors doped with a color center.
6. If these tests are successful, we can foresee future construction of I.R. detectors used as new particle detector devices such as I.R. calorimeters, gamma spectrometers, and light signal amplifier of the drifting electrons.
7.

ACKNOWLEDGEMENTS

The author is especially indebted to E. Conti for his continuous help and advise during the beam time run at the Legnaro National Lab. I would like to thank A. Meneguzzo, F. Borghesani, G. Bressi, P. Calvani, and D. Zanello for stimulating discussions on the subject.

REFERENCES

1. P. Lindblom, O. Solin, NIM A268 (1988) 204.
2. R. D. Andersen et al., NIM 140 (1977) 371.
   A. Policarpo et al., NIM 102 (1972) 337.
3. Masuda et al., NIM 160 (1979) 239.
4. II - VI Incorporated, PA, USA.
5. E.G.G. Judson Optoelectronics; Hamamatsu Ind.; Fermionics IR Ind.
6. Hamamatsu Infrared Technical Information.
7. E. Dereniak, D. Crowe; Optical Radiation Detectors; Wiley & Sons (1984).
8. Optics-Handbook, VOL. I, (15).
9. E.G.G. Judson Optoelectronics, I.R. Detector.
10. D. C. Lorents Physica, 82 C (1976) 19.
11. H. A. Köhler et al., Phy. Rev. A 9, 2 (1974) 768.

99-03-076

AEROGEL AND ITS APPLICATIONS TO RICH DETECTORS

E. Nappi
INFN, Sez. Bari, Istituto Nazionale di Fisica Nucleare, via Amendola 173, I-70126 Bari, Italy

ABSTRACT

Beam test results show that the "new generation" aerogel has attractive features and appears an interesting candidate as radiator in Ring Imaging Cherenkov (RICH) detectors. The challenging applications envisaged in the LHCb experiment at CERN and in the HERMES experiment at DESY will be reviewed.

1 Introduction

The hadron identification in the momentum domain of few GeV/c represents a challenge for Cherenkov detectors, in fact traditional gas and liquid radiators have a refractive index either smaller of 1.0018 (C_5F_{12}) or larger than 1.27 (liquid C_6F_{14}). To avoid the use of gases at high pressure or in unmanageable liquified form, the only possible way to partially close the gap in refractive indices is represented by silica aerogel that can be produced in a fairly wide range from $n = 1.004$ to $n = 1.1$. After the unsuccesful attempt of Linney and Peters [1] in 1972 to use compressed silica powder to obtain a material with n<1.2, soon abandoned due to the very poor transparency of their radiators, in 1973 Cantin *et al.* [2] adopted silica aerogel in Cherenkov counters. Although aerogel was discovered in 1931 [3], a time and cost effective fabrication method was found only in the late 1970s, when France decided to store rocket fuels in porous materials. Since then, an explosive growth of specific application in the scientific community has stimulated new techniques for the production of aerogel with remarkable optical quality. Indeed aerogel is now currently produced in a sol-gel chemical process that provides a very transparent hydrophobic polymer gel structure while old aerogel was fabricated in a way to lead to seedy hydrophillic colloidal structures. The "breakthrough" in aerogel fabrication promoted more advances in the use of this material in Cherenkov detectors, as V.I. Vorobionov [4] and H. v. Hecke [5] pointed out in 1991 and 1993, respectively. Nonetheless, the major merit of the rapid progress of aerogel in real RICH devices must be ascribed to J. Seguinot and T. Ypsilantis, who revised the van Hecke proposal in the light of currently

available photodetector technology and envisaged an appealing application in the LHCb experiment [6]. The outstanding potential of their detector design inspired the upgrade of HERMES at DESY [7].

In the next section, the chemical and physical properties of silica aerogel will be briefly reviewed, results from beam tests at CERN-PS are then presented in Sec. 3. An outlook of the experiments LHCb and HERMES will be given in Secs. 4 and 5, respectively. Finally, Sec. 6 is devoted to conclusions.

2 Chemical and Physical Properties of Silica Aerogel

Aerogel is a manmade material that could have a density as low as three times that of air. It essentially consists of grains of amorphous SiO_2 with sizes ranging from 1 to 10 nm linked together in a three-dimensional structure filled by trapped air. The huge number of such tiny primary particles determines an internal surface close to 1000 m^2/g that plays the fundamental role in the aerogel chemical and physical behavior. It exists a simple relationship between the resultant index of refraction and the aerogel density ρ in g/cm^3 [8]:

$$n = 1 + 0.21\ \rho. \tag{1}$$

Density values lying between 0.003 g/cm^3 and 0.55 g/cm^3 are in principle available, corresponding to refractive indices of n=1.0006 ($\gamma_{threshold} = 29$) and n=1.11 ($\gamma_{threshold} = 2.3$), respectively.
In the aerogel preparation, the starting phase is the hydrolysis and condensation of silicon alkoxides in presence of an alcoholic solvent. Aerogel is then obtained by removing the solvent in a quite complicated way because if the liquid were simply left to evaporate, then adhesion and capillary forces would shrink the gel into a very dense material. Therefore, in order to prevent the collapse of the porous structure, the pressures and temperatures during liquid extraction must be raised above the triple point of the solvent. In the past, this operation required high temperatures and high pressures. Moreover, the demanding control of the correct quantity of solvent made possible only the production of silica aerogel within a limited range of refractive indices [8].

In the final treatment, the aerogel needed to be baked at several hundred degrees Celsius in order to dry off the residual adsorbed solvent. The final product had surfaces not particularly clean and flat and the baking treatment makes it very hydrophillic, consequently aerogel samples used in the experiments had to be often rebaked during their operative life.

In 1988, a new fabrication process was developed at Lawrence Livermore National Laboratory, later on adopted by the russian team lead by A. P. Onuchin in collaboration with the Boreskov Institute of Catalysis in Novosibirsk to produce very transparent silica aerogel with refractive index in the range 1.005–1.055 [9].

Oppositely to the aforementioned method, called "one-step," the new one treats the starting gel into two succesive steps: the alcohol (mainly methanol) within the gel is, in the first step, replaced by liquid

CO_2 that undergoes a supercritical drying in the second step without damaging the aerogel [10]. The "two-step" process is much safer than the simply extraction of supercritical methanol, in fact CO_2 has a lower critical point (31°C and 1050 psi) than methanol (240°C and 1600 psi) and does not pose an explosion hazard as alcohol does.

But the breakthrough in the fabrication process occured only few years ago, in the framework of the Belle experiment at the B-factory in Japan, when silica aerogel with very low refractive index was produced by means of a revolutionary technique [11]. The National Laboratory for High Energy Physics (KEK) in Japan in collaboration with Matsushita Electric Works developed a method based on the old single-step process but adopting the basic philosophy of the two-step method. The aerogel is baked under supercritical conditions after replacing the alcohol with CO_2 by avoiding in this way the complication of the alcohol distillation. This aerogel is hydrophobic, due to a treatment of the surface of the aerogel pores, and highly transparent, but it loses this property if a baking process is applied to improve its transmittance.

Moreover, KEK aerogel has been found to be radiation hard at least up to 9.8 mrad of gamma ray dose [12].

2.1 Optical Properties

The granular structure of aerogel with a typical length scale of few nm determines its optical properties. Indeed, the behavior of visible light in aerogel is dominated by Rayleigh scattering which increases as the fourth power of the frequency. The bluish haze that surrounds aerogel samples is an effect of the Rayleigh scattering since short wavelengths are the most severely affected by the continuos scattering mechanism. The internal absorption does not play a significant role in the visible region (the intensity drops to 1/e only after several cm), while weak absorbances appear in the infrared. The measured transmittance t of an aerogel sample of thickness L, as function of the light wavelength λ in the range from 300 nm to 700 nm, is fairly fitted by the expression:

$$t = Ae^{-CL/\lambda^4}, \tag{2}$$

where C characterizes the aerogel clarity, and A is the measured transmission in the long-wavelength region. Samples with a good optical quality have A and C close to the value of 1 and 0 respectively. The typical values of the parameters A and C have been reported in Table 1 where samples with $n = 1.03$ produced with the aforementioned fabrication methods are compared.

When the Rayleigh scattering occurs, the directionality of the Cherenkov radiation is completely lost. Therefore, the major concern associated with the design and construction of a RICH detector with an aerogel radiator is whether the Cherenkov photons that traverse the aerogel without any scattering are in sufficient number to allow the measurement of their emission angle with the expected accuracy.

Table 1: Silica aerogel optical parameters

Fabrication method	Producer	A	C ($\mu m^4 cm^{-1}$)	Ref.
"One-Step"	Airglass Co. (Sweden)	0.96	0.018	[13]
"Two-Step"	Jet Propulsion Lab (USA)	0.96	0.012	[6]
"Two-Step"	Boreskov Institute of Catalysis (Russia)	0.96	0.005	[14]
"KEK Method"	KEK Lab. (Japan)	0.96	0.0085	[15]

The fraction N of photons of wavelength λ that cross undeflected an aerogel sample of thickness L, characterized by the optical parameters A and C, is given by:

$$N = A\lambda^4(1 - e^{-CL/\lambda^4})/CL. \tag{3}$$

Although the C parameter of Russian samples is smaller than that of aerogel samples fabricated with other methods, the KEK aerogel has the big advantage to be hydrophobic and therefore it ages less in the long term. By assuming the best optical parameters, the fraction of photons of 350 nm that have not undergone any scattering inside a 3 cm thick sample is about 60%, but N raises up to almost 85% for photons of 500 nm.

These simple calculations show that the useful production of Cherenkov light is limited to the visible. This therefore places high demands on photon detection. A large area multicell hybrid photodiode (HPD) with a bialkali photocathode seems the most promising candidate to detect and resolve single photoelectrons from aerogel [6]. Moreover, HPDs ensure operational stability on a long term since they are devices without intrinsic gain [16].

3 Beam Test Results

In the framework of Hermes and LHCb RICH detector development, investigations have been carried out to prove the feasibility of detecting a single event Cherenkov ring produced in aerogel [17].
Aerogel samples with n=1.03, procured from KEK, were tested at the PS-T9 beam facility at CERN with 10 GeV/c negative pions.
The experimental setup is schematically shown in Fig. 1. It consists of a black painted light-tight aluminum box flushed with nitrogen at atmospheric pressure, which contains the aerogel sample and an angled spherical mirror used to focalize the light from the radiator on the photodetector entrance window. The mirror has a focal length of 45 cm, and thus, aerogel rings with a diameter d of 11 cm are expected in the mirror focal plane. Smaller rings, with $d \sim 2$ cm, are instead produced by particles in nitrogen between the aerogel and the mirror. Two different systems employing either a single phototube (PM) or a matrix of 114 phototubes have been used to detect the emitted light.

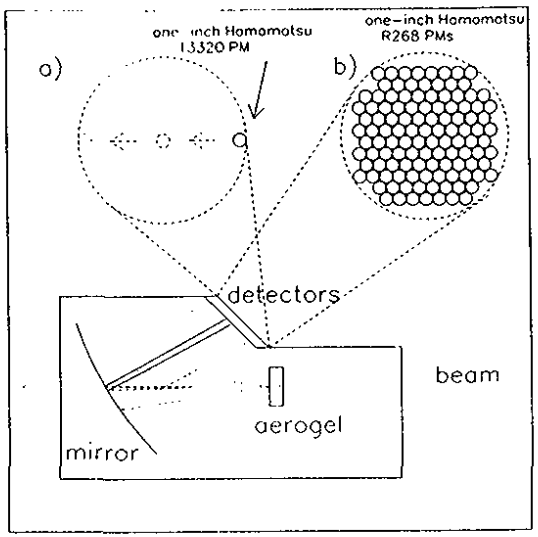

Figure 1: Schematic layout of the test setup at CERN for the imaging of the Cherenkov light produced in silica aerogels with n=1.03. Two detector schemes were consecutively implemented on the mirror focal plane: (a) a single phototube mounted on a motorized stage, and (b) an array of 114 photomultipliers.

In the first part of the test, a Hamamatsu 1332Q PM with a bialkali photocathode of one inch was installed on a linear motorized translator in order to scan horizontally across the mirror focal plane. The number of counts, referred to the same number of triggers, registered by the PM during the scanning of the focal plane, is reported in Fig. 2 as a function of the position. In order to suppress the noise and mantain sensitivity to single photoelectrons, a threshold in the pulse height was placed between the pedestal and the one-photoelectron (*p.e.*) peak of the PM spectrum. The stronger peak in Fig. 2, obtained with the PM nearly in the center of the focal plane, corresponds to the Cherenkov ring produced in nitrogen. Another peak is clearly visible when the PM is displaced 11.6 cm from the position of the maximum of the first peak. The same enhancement is seen moving the PM in the opposite direction. These enhancements are originated from the unscattered Cherenkov light produced in the radiator and prove that KEK aerogel preserves the direction of an appreciable fraction of Cherenkov photons. From the values of the mirror focal length and from the observed radius of the aerogel ring, a refractive index of 1.03 has been calculated, in good agreement with the nominal value provided by the KEK group (n=1.028). The resolution of the peaks in Fig. 2 is dominated by the size of the PM photocathode.

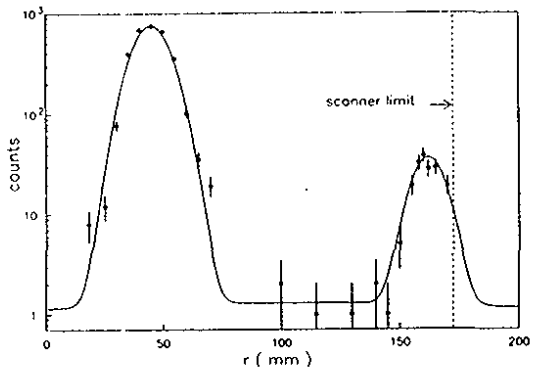

Figure 2: Scan with one PM across the mirror focal plane. The first peak, on the left-hand side, is due to the unresolved Cherenkov ring from nitrogen, while the second peak corresponds to Cherenkov photons produced in the aerogel. The counts between the two peaks are very few as expected.

In the second part of the test, the array of 114 one-inch PM's allowed to perform the electronic imaging of the full Cherenkov pattern. A threshold was applied to the signal of each of the 114 PM's recorded, corresponding to about 2σ of the pedestal distribution.
In Fig. 3, the PM hit map containing a large number of overlapped events is reported. The nitrogen and aerogel rings are clearly visible over a very low background.

From the positions and the number of PM's fired in each event, the average radius of the ring, the average number of Cherenkov photoelectrons per ring and the average background due to photons emerging from the aerogel after having undergone one or more scatterings, were calculated [17]. The following results, referred to a 2.5 cm thick sample, were found:
(1) a ring radius value of 11.4 ± 0.5 cm;
(2) an average number of 14.9 *p.e.* per ring; and
(3) an average background of 2.4 *p.e.* per ring.

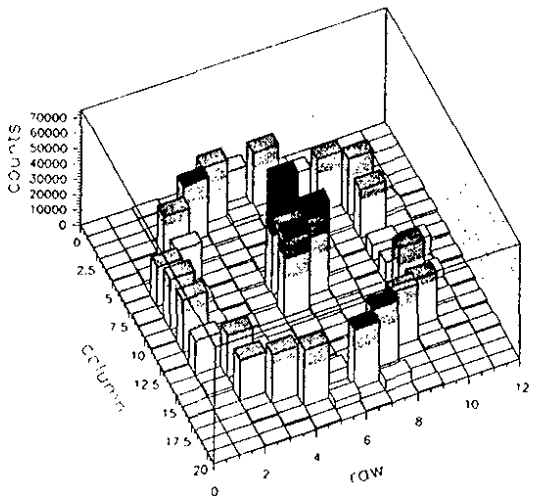

Figure 3: The photomultiplier hit map over the mirror focal plane obtained by overlapping events from a full run. The Cherenkov ring from aerogel is clearly visible, while the ring from nitrogen is poorly resolved by the three central photomultipliers. The sparse background hits show the good optical quality of the tested aerogel sample.

4 THE LHCb EXPERIMENT AT CERN

LHCb is an experiment designed to study CP violation in B decays. It is conceived as a collider-mode forward spectrometer which will be operational at the LHC start-up. The proposed layout (Fig. 4) features an accurate momentum reconstruction and particle identification since precision determination of the CKM unitarity triangle angles requires an excellent pion/kaon separation over the momentum range from 1 GeV/c to 150 GeV/c. A detailed description of LHCb can be found in Ref. [18], in the following only those aspects of the setup which concern particle identification will be addressed.

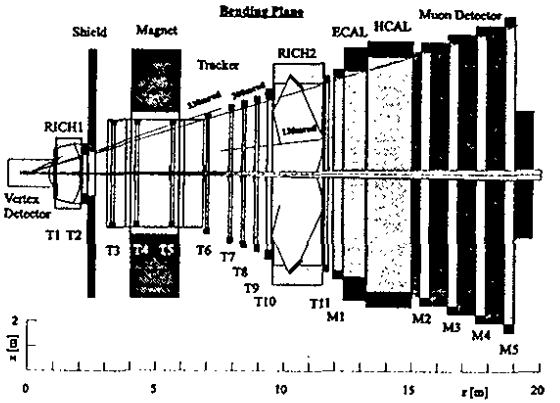

Figure 4: LHCb layout.

The desired momentum range for pion/kaon separation cannot be spanned by one refractive index setting; therefore, two focused RICH detectors with three radiators have been proposed. The first RICH is placed upstream the dipole magnet to allow the identification of particles in the low momentum region from 1 to 60 GeV/c. It is based on the innovative idea to implement aerogel and C_4F_{10} radiators in the same focusing system by positioning the aerogel radiator close to the gas vessel entrance window and tilting the 2 m focal length mirror to bring the image out of the beam aperture in order to reduce secondary interactions. Photons are detected via an array of HPDs located on each side of the RICH detector (Fig. 5). The second RICH has a 2 m long CF_4 gas radiator to identify high momentum particles between 16 and 150 GeV/c. A system of mirrors transfers the ring images to the HPD array located in such a way that it is not traversed by particles.

Anticipated performances of the RICH systems are listed in Table 2. The particle identification layout

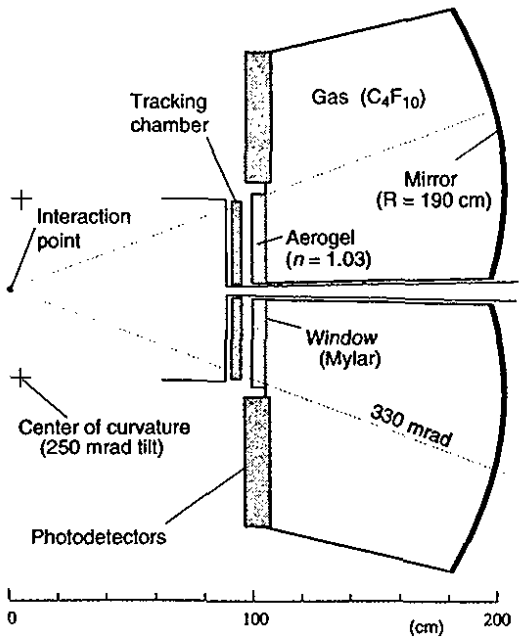

Figure 5: The innovative set-up of the LHCb RICH with aerogel and gas radiators.

proposed has a high discrimination power, but the innovative technical solution envisaged need crucial tests to determine their feasibility.

5 The HERMES Experiment at DESY

Hermes is an internal gas-target experiment designed to investigate the nucleon spin structure functions at HERA [19]. An open spectrometer has been built with the aim to measure the scattered electron and the leading hadrons coming from the target fragmentation with a momentum and angle resolution of 1% and 1 mrad (at 4 GeV/c), respectively.

Table 2: Expected performances of LHCb RICH detectors with n=1.03 aerogel radiator and CF_4, C_4F_{10} gas radiators. The following factors are listed: momentum thresholds for pions and kaons, maximum Cherenkov emission angle, contributions to the angle resolution from the uncertainty of the photon emission-point, from the radiator chromatic dispersion and from photon detector spatial resolution (assuming 2.5x2.5 mm^2 pixel size), total angle resolution per photoelectron, and the momentum upper limit of $3\sigma_{\pi/K}$ separation.

n	1.03 (aerogel)	1.0005 (CF_4)	1.0014 (C_4F_{10})
$p_{tresh,\pi}$ (GeV/c)	0.6	4.5	2.7
$p_{tresh,K}$ (GeV/c)	2.0	15.6	9.4
θ_C (mrad)	240	30	53
$\sigma_\theta^{emission}$ (mrad)	0.4	0.2	0.6
$\sigma_\theta^{chromatic}$ (mrad)	1.2	0.3	0.6
σ_θ^{pixel} (mrad)	0.7	0.2	0.7
σ_θ^{total} (mrad)	1.5	0.4	1.1
p_{max} (GeV/c)	20	146	73

The spectrometer consists of a conventional dipole magnet of 1.3 Tm and many tracking chambers for an accurate event reconstruction (Fig. 6). The scattered primary electron is identified with an efficiency greater than 97% (with less than 1% of hadron contamination) by the combination of a lead-glass calorimeter, a preshower, and a transition radiation detector. The threshold Cherenkov detector that formerly allowed the identification of pions above a threshold of 3 GeV/c using C_4F_{10} was replaced by a LHCb-like dual radiator RICH during the summer of 1998 [20].

In this way, the unique opportunity to provide valuable information on the flavor dependence of the spin structure functions and estimates of the strange sea polarization is fully exploited by an unambiguous identification of pions, kaons, and protons in the momentum range from 3 to 20 GeV/c.

6 Conclusions

Hydrophobic, crack-free, very transparent aerogel samples are now routinely fabricated. Loss of photons due to the absorption and scattering processes in the bulk material have been minimized by using innovative production techniques. Aerogel ageing effects due to exposure to atmosphere can be alleviated by proper handling and storage. This new silica aerogel can be an ideal medium to be employed in RICH detectors as radiator. Test beam studies of aerogel gave very promising results indicating that KEK-aerogel has the required optical quality, and therefore, it is suitable to be used for RICH detectors. Moreover results show that the background from scattered photons is low.

LHCb and HERMES experiments have already planned to implement an aerogel RICH in their setup. Indeed, a RICH device with aerogel and an array of visible light photodetectors shows an attractive con-

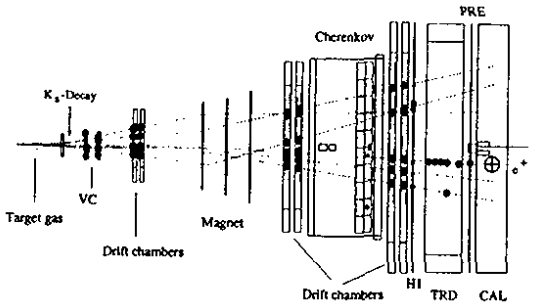

Figure 6: Reconstruction of an event in the HERMES spectrometer. The scattered positron has been recognized by hits in the transition radiation detector (TRD), the preshower counter (PRE) and the electromagnetic calorimeter (CAL).

ceptual simplicity due to the modest service and maintenance needs. The major drawback of this technique is the high detector cost per unit of surface. In fact, the commercial available devices (HPD and multi-anode photomultipliers) have suitable performances but they suffer of large inactive area and high cost. The developments of cheap hybrid phototubes with large active area is underway at CERN in collaboration with INFN-Bari and ISS-Rome [21].

References

[1] A. Linney and B. Peters, Nucl. Instr. Methods **100** (1972) 545.

[2] M. Cantin *et al.*, Nucl. Instr. Methods **118** (1974) 177.

[3] S. S. Kistler, J. Phys. Chem. **34**, (1932) 52.

[4] V. I. Vorobionov *et al.*, *Proceedings of the Workshop on Physics and Detectors for DAPHNE*, report INFN-Frascati, 1991.

[5] H. van Hecke, Nucl. Instr. Methods A **343** (1994) 311.

[6] J. Seguinot and T. Ypsilantis, Nucl. Instr. Methods A **368** (1995) 229.

[7] R. De Leo *et al.*, "Proposal to add a ring imaging Cherenkov detector to HERMES," INFN-ISS 96/9 and E. Cisbani *et al.*, "Progress report on the feasibility studies of a RICH detector for HERMES," INFN-ISS 96.

[8] G. Poelz and R. Reithmuller, Nucl. Instr. Methods **195** (1982) 491.

[9] A. R. Buzykaev *et al.*, Nucl. Instr. Methods A **379** (1996) 465.

[10] T. M. Tillotson and L. W. Hrubesh, UCRL-Ext., Abs. 102517, LLL (1990).

[11] I. Adachi *et al.*, Nucl. Instr. Methods A **355** (1995) 390.

[12] S.K. Sahu *et al.*, Nucl. Instr. Methods A **382** (1996) 441.

[13] D. E. Fields *et al.*, Nucl. Instr. Methods A **349** (1994) 431.

[14] E. Kravchenko, "Measurement of optical parameters of the aerogel," talk presented at the *Third International Workshop on Ring Imaging Cherenkov Detectors*, Ein-Gedi, November 1998 (Proceedings will be published in Nucl. Instr. Methods).

[15] R. De Leo *et al.*, "Optical characterization of n=1.03 silica aerogel from Matsushita, submitted to Nucl. Instr. Methods A.

[16] R. De Salvo, Nucl. Instr. Methods A **315** (1992) 375.

[17] R. De Leo *et al.*, Nucl. Instr. Methods A **401** (1997) 187.

[18] LHCb Technical Proposal CERN/LHCC98-4.

[19] K. Ackerstaff *et al.*, Nucl. Instr. Methods A **417** (1998) 230.

[20] E. Cisbani *et al.*, Proposal for a dual radiator RICH for HERMES, HERMES internal note 97-003 (March 1997).

[21] A. Go *et al.*, "Development of RICH detector and large-area HPD for LHCb experiment," talk presented at the *Third International Workshop on Ring Imaging Cherenkov Detectors,* Ein-Gedi, November 1998 (Proceedings will be published in Nucl. Instr. Methods).